CONF-9605109--1

LA-UR-96- 0250

TITLE: OBSERVATIONS OF MAGNETOSPHERIC SUBSTORMS OCCURRING WITH NO APPARENT SOLAR WIND/IMF TRIGGER

AUTHOR(S): M. G. Henderson
G. D. Reeves
R. D. Belian
J. S. Murphree

BMITTED TO: ICS-3 SUBSTORM CONFERENCE
May 13-17, 1996
Versailles, France

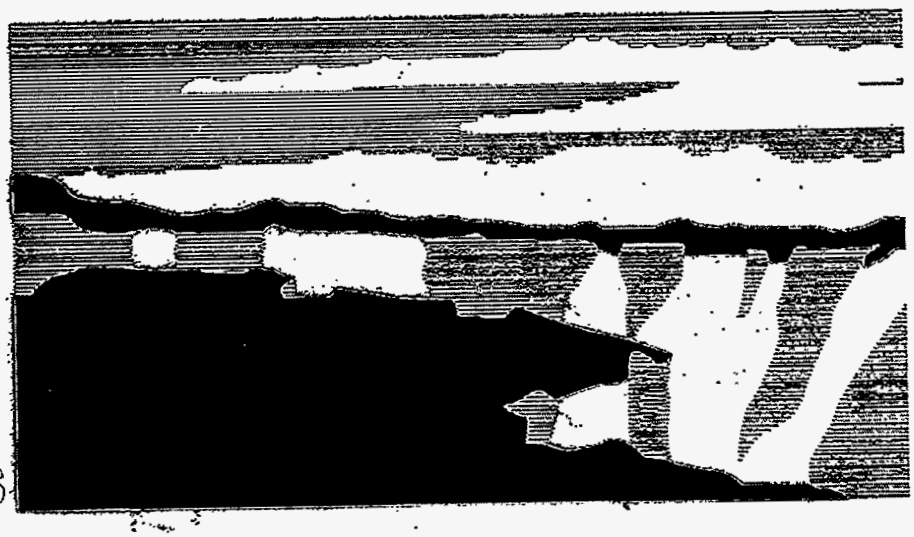

Los Alamos
NATIONAL LABORATORY

AGU JGR galley style, v3.1, 14 Feb 94

Observations of magnetospheric substorms occurring with no apparent solar wind/IMF trigger

M. G. Henderson, G. D. Reeves and R. D. Belian

Los Alamos National Laboratory, Los Alamos, New Mexico

J. S. Murphree

University of Calgary, Calgary, Alberta

Abstract. An outstanding topic in magnetospheric physics is whether substorms are always externally triggered by disturbances in either the interplanetary magnetic field or solar wind, or whether they can also occur solely as the result of an internal magnetospheric instability. Over the past decade, arguments have been made on both sides of this issue. *Horwitz* [1985] and *McPherron et al.* [1986] have shown examples of substorm onsets which they claimed were not externally triggered. However, as pointed out by *Lyons*, [1995a,b] there are several problems associated with these studies that make their results somewhat inconclusive. In particular, in the McPherron et al. study, fluctuations in the B_y component were not considered as possible triggers. Furthermore, Lyons suggests that the sharp decreases in the AL index during intervals of steady IMF/solar wind, are not substorms at all but rather that they are just enhancements of the convection driven DP2 current system that are often observed to occur during steady magnetospheric convection events. In the present study, we utilize a much more comprehensive dataset (consisting of particle data from the Los Alamos energetic particle detectors at geosynchronous orbit, IMP 8 magnetometer and plasma data, Viking UV auroral imager data, mid-latitude Pi2 pulsation data, ground magnetometer data and ISEE1 magnetic field and energetic particle data) to show as unambiguously as possible that typical substorms can indeed occur in the absence of an identifiable trigger in the solar wind/IMF.

Introduction

The first observations to show a positive correlation between geomagnetic activity and the direction of the interplanetary magnetic field (IMF) were made by *Fairfield and Cahill* [1966] using data from the Explorer 12 spacecraft together with data from several ground-based magnetometer stations. The results of that study (and of numerous other studies conducted over the decades since) show that geomagnetic disturbances tend to occur when the IMF is directed southward while intervals of relative calm result when the IMF is directed northward indicating that the transfer of energy from the solar wind to the Earth's magneto-

Paper number .

sphere is more efficient when the IMF B_z component is negative. Therefore, extended intervals of -B_z can lead to a build up of energy in the magnetosphere which is typically (although not always) dissipated episodically in the form of substorms. Although the precise nature of the physical mechanism (or mechanisms) responsible for the substorm expansion phase is still a topic of considerable on-going debate, it is reasonably well established that the onset of a substorm can frequently be related to disturbances in the solar wind and/or IMF.

Early on it was recognized that sudden changes in the direction of the IMF could trigger the expansion phase of substorms [*Pudovkin et al.*, 1970; *Aubry and McPherron*, 1971; *Burch*, 1972, 1973] – particularly when the IMF B_z component was directed southward for some time beforehand. Later, using superposed epoch analysis techniques, *Caan et al.* [1975, 1977, 1978] showed that, in particular, substorm onsets tend to be triggered by northward turnings of the IMF (see also *Foster et al.* [1971]). And additional support for these results has been provided by *Rostoker et al.* [1982], *Pellinen et al.* [1982], *Rostoker* [1983] and *Rostoker et al.* [1983] who examined individual events in more detail. As well, *Kokubun* [1977], showed that substorm onsets could also be triggered by magnetospheric compressions due to sudden changes in the solar wind dynamic pressure – provided that the magnetosphere was already in a meta-stable state (e.g. during the growth phase) prior to the arrival of the disturbance. And, to complicate matters, *Troshichev et al.* [1986] pointed out that many substorm onsets which were apparently triggered by northward turnings of the IMF were also accompanied by sudden directional changes in the azimuthal component and they showed that such perturbations (particularly when B_y turns from positive to negative values) could also trigger onsets by themselves. A statistical survey of the relative occurrence frequency of a variety of triggering disturbances was compiled for a 6 month interval by *McPherron et al.* [1986] and it was determined that northward turnings of the IMF were responsible for triggering $\approx$45% of the onsets while $\approx$29% of them occurred when the IMF B_z was steadily southward and only $\approx$2% of the onsets were triggered by pressure pulses. However, their results did not allow for the possibility of onsets triggered by sudden changes in the azimuthal component of the IMF. Inclusion of this additional category of potential triggers would quite probably have altered their results significantly.

Despite these complications, the fact that onsets can be triggered by disturbances in the solar wind and IMF

is quite well established and there appears to be little doubt that many substorms are indeed triggered in this manner. Nevertheless, *Horwitz* [1985] and *McPherron et al.* [1986] showed that substorm onsets could also occur in the absence of major directional changes in the IMF. These observations are significant because they suggest that substorms can also occur as the result of a purely internal magnetospheric instability. These observations are significant because they have important implications for substorm theories. Recently, however, the results of McPherron et al. have been called into question by Lyons [1995a, 1995b] who claims that one of their events actually is triggered by a reduction in B_y while another one is likely not a substorm at all but is rather caused by some other type of disturbance (although no evidence to support this claim is offered by Lyons). While it is important to note that Lyons' objections to the conclusions of McPherron et al. are primarily motivated by a desire to reconcile their observations with his recently proposed substorm model which requires a sudden reduction in the externally imposed solar wind electric field, some of the objections he raises are valid and also apply to the Horwitz study.

In the Horwitz study, the timing of the expansion phase onsets at Earth were determined solely on the basis of sharp perturbations in the AL and AE indices – a technique which is often unreliable, particularly during intervals of steady magnetospheric convection (SMC) (or convection bays) which occur when the IMF B_z-component is directed southward for extended periods of time. *Kokubun et al.* [1977] found that during such times, large disturbances in ground based magnetograms could occur that were not the result of substorm activity but rather appeared to be due to enhancements of the DP-2 current system which is driven by magnetospheric convection. Furthermore, one of the events (the September 10, 1979 case) presented by Horwitz (see his figure 1), actually does show small but significant directional changes in the B_y and B_z components that could be associated with the onset. Note that although this northward turning does not coincide precisely with the abrupt increase in the AE index, the use of a nominal time delay of 1 hour between ISEE 3 and the Earth in that study could be off by as much as $\pm$15 minutes depending on what the solar wind speed was.

In the McPherron et al. study, although IMF data from the (much closer) IMP 8 spacecraft were used together with the solar wind dynamic pressure, none of the three examples presented convincingly show that the onset occurred without an identifiable solar wind/IMF

trigger. The main reason for this is that they neglected to analyze the B_y component for possible signs of a trigger, but ambiguities also exist in the substorm identification process because they also relied solely on sharp perturbations in the AL or AE indices. The three events shown in the McPherron et al. study are reproduced in figure 1 along with additional data not presented in the original study. From top to bottom, the panels in the stacked plots show: the three components of the interplanetary magnetic field vector in GSM coordinates as measured by the IMP8 spacecraft, the field magnitude, the solar wind dynamic pressure (nmV^2) and the AU and AL indices. The location of the IMP 8 spacecraft is shown in GSM coordinates at the bottom of each plot. The solid black points on the dynamic pressure plot represent values from the Los Alamos plasma instrument while the open points connected by straight line segments represent values of the solar wind dynamic pressure derived from the MIT plasma instrument. We note that the large single-point increases in the MIT values for the April 3, 1978 event are probably spurious but have been retained for completeness.

A re-examination of the three events shown in the McPherron et al. study reveal the following observations. For the April 3, 1978 case, it can be seen that; 1) although the B_z component is relatively smooth compared to typical cases, all three components (including the B_y component) show significant rapid fluctuations just prior to the onset (at 12:10 UT), and 2) the B_y and B_x components show small but clear directional changes just prior to the onset. Note that if the isolated spikes in the MIT plasma data are neglected, the solar wind dynamic pressure was fairly steady at the time of onset and was therefore not a likely trigger for the substorm. For the January 15, 1978 case, none of the IMF components are very smooth but more importantly, the onset (at 10:30 UT) is closely associated with a rather large directional change in the B_y component. (There was no pressure data available for this event.) For the March 31, 1978 event, although the solar wind dynamic pressure is steady, the magnetic field components are quite disturbed and show many small but significant directional changes before and after the onset at 11:15 UT. These fluctuations cannot convincingly be ruled out as possible triggers for the substorm.

The ambiguities which are raised by a more complete analysis of these events therefore casts some doubt on the assertion that some substorms are the result of a purely internal magnetospheric instability. The purpose of this paper is to re-assert as unambiguously as possible that magnetospheric substorms can indeed occur in

the absence of an identifiable trigger in the IMF/solar wind. To show this, a comprehensive set of observations from multiple locations in the magnetosphere and on the ground are presented for six different substorms.

Observations

Rather than relying solely on sharp decreases in the AL index or sharp increases in the AE index as indicators of substorm onset, the events presented here were initially identified as substorms based on multi-point observations of energetic particle injections at geosynchronous orbit provided by the Los Alamos energetic particle detectors. Data from a total of six geosynchronous spacecraft are used in the present study. Four of them (1982-019, 1984-037, 1984-129, and 1987-097) were equipped with CPA (Charged Particle Analyzer) detectors and two of them (1989-046 and 1990-095) were equipped with SOPA (Synchronous Orbit Particle Analyzer) detectors. The differential energy bands corresponding to the six lowest energy electron channels for each of these detectors are shown in table 1. For each of the cases, the solar wind dynamic pressure (nmV^2) was computed from the plasma parameters determined by the Los Alamos plasma instrument onboard the IMP8 spacecraft and the interplanetary magnetic field components were measured by the fluxgate magnetometer also onboard the IMP8 spacecraft.

The primary initial selection criteria were such that: 1) the energetic particle data had to show typical signatures of an injection, including the observation of dispersed drifting populations away from midnight. 2) in a qualitative sense, both the solar wind dynamic pressure and the B_y and B_z components of the interplanetary magnetic field at IMP 8 were required to remain steady for at least 30 minutes prior to the onset. We note that fluctuations in B_x were not considered to be as important since changes in that component do not lead to changes in the electric field as do changes in the B_y and B_z components. Nevertheless, all but one of the cases shown here occurred when B_x was also very steady. 3) the IMP 8 spacecraft was required to be located approximately within $\pm 45°$ of the noon-midnight meridian in order to reduce problems associated with spatial variability of the IMF in the azimuthal direction. Of the six events shown here, four of them were closer than 20° to the noon-midnight meridian and five were closer than 25°.

Although many events were found which meet these criteria, the final selection of events for inclusion here was primarily motivated by the fact that digital ground

magnetometer data (including Pi2 pulsation data) was readily accessible for them. Table 2 shows a list of the six events (with dates and onset times) that were ultimately chosen. The first two events occurred during the 1986 PROMIS campaign while the third event occurred during the Viking era and the last three events occurred during the first two years of the STEP project (1990 and 1991). The locations and station codes for the ground magnetometer stations used in this study are shown in table 3.

April 14, 1986

Multi-point observations of an isolated substorm which occurred on April 14, 1986 are presented in Figure 2. From top to bottom, the panels in the stack plot show: the energetic electron fluxes measured by the Los Alamos energetic particle detectors at three different locations in geosynchronous orbit, the AL index, the three components of the interplanetary magnetic field vector in GSM coordinates (from the fluxgate magnetometer onboard IMP 8), the solar wind dynamic pressure (from the Los Alamos plasma instrument onboard IMP 8), Pi1– and Pi2–filtered high resolution H component magnetometer data from the Kakioka midlatitude ground station, the 1.4–1.6 keV proton fluxes at ISEE1 and the tail field inclination angle at ISEE1 ($\tan^{-1}(B_z/B_x)$) The universal time (in hours) is given along the bottom axis along with the corresponding magnetic local times of the Los Alamos geosynchronous satellites and the locations of the IMP 8 and ISEE 1 spacecraft in GSM coordinates. The dashed lines (drawn at 1105:06 UT) represent the main onset time as determined by the Pi1 and Pi2 pulsations at Kakioka. In the panels displaying parameters measured at IMP 8, these lines have been shifted to account for the time delay between IMP 8 and the dayside magnetopause which was calculated based on the plasma parameters at IMP 8 and the location of the magnetopause as determined by the formula of *Petrinec and Russell* [1995].

From this figure it can be seen that there was a clear onset at approximately 11:05 UT. At satellite 1984-129, the energetic electron fluxes increased dramatically at about this time and were dispersed slightly indicating that it was close to but east of the injection region. At 1982-019 and 1984-037, which were located progressively farther to the east, the amount of energy dispersion had increased considerably and after $\approx$12 UT, a very dispersed increase in the fluxes at 1984-129 was observed. This behavior is indicative of a drifting electron population produced by the injection on the nightside which had been circulated completely around the

earth to produce a drift echo at 1984-129. We note also, that there was some activity prior to this at 1984-129 beginning at about 1015 UT that was also associated with weak enhancements in the Pi2 pulsations, although the AL index did not register any major perturbations between this time and the time of the main onset at 1105:06 UT. These "precursors" were likely due to pseudo-breakup activity (see Koskinen et al. [1992] for a description of the characteristics of pseudo-breakups) occurring prior to the onset of the main auroral expansion phase. In the lowest panel, it can be seen that the tail field inclination at ISEE1 (which was close to apogee and was situated near the noon-midnight meridian plane) decreased substantially over the time period leading up to the onset, indicating that the tail field was considerably stretched at that time. As well, beginning at about 1030 UT, the 1.4–1.6 keV proton fluxes at ISEE 1 show the occurrence of a series of plasma sheet dropouts and recoveries prior to the main onset at 1105:06 UT and again these are probably related to the pseudo-breakup activity.

Figure 3 shows the H– or X–component magnetometer data from 29 ground stations distributed throughout the world. The traces have been divided up into three separate groups corresponding to the polar cap region, the auroral zone and the mid-latitude regions. Within each of these groups the stations have been organized such that the magnetic longitude decreases (relative to the first stations in each group) from top to bottom. The black filled circles above some of the curves denote the time at which the corresponding station crossed the local magnetic midnight meridian while the open circles denote the times at which the corresponding stations crossed the local magnetic noon meridian. As shown, the substorm disturbance at approximately 1105 UT was localized to the night-side sector in both the auroral zone and at mid-latitudes and produced a weak increase in the H-component of only one of the polar cap stations. Thus, the ground magnetic perturbations during this event are consistent with what is typically observed during substorms and are not consistent with a global enhancement of the convection driven DP2 current system.

Finally, in Figure 4 we present a sequence of Viking ultraviolet auroral images showing the development of the northern auroral distribution during this event. All of the images shown were acquired with camera 0 which is sensitive to the Lyman-Birge-Hopfield band emissions of N_2 (the passband of the camera is approximately 134 - 180 nm). Although the sequence of images shown do not overlap with the onset time (at 1105:06 UT), they

do span a significant portion of the recovery phase of the substorm and clearly show the presence of classical recovery phase signatures including a bright wavy arc system at the poleward edge of an expanded and relatively dark bulge.

Taken together, these observations establish unambiguously that this event was indeed a classical magnetospheric substorm. Interestingly, however, during this entire interval all three components of the IMF (as shown in the fifth sixth and seventh panels of Figure 2) remained quite steady with no readily identifiable perturbation that could reasonably be construed as a potential trigger for the substorm. The same is true when one examines the solar wind dynamic pressure.

April 13, 1986

Multi-point observations of a substorm which occurred on April 13, 1986 are presented in figure 5. The format of the plot is identical to that of figure 2. As shown, the energetic electron fluxes at 1984-129 suddenly increased just before 11 UT and remained elevated for a few hours afterward. This abrupt increase was also observed later on as drifting dispersed populations at 1982-019 and 1984-037 which were situated progressively farther to the east of the midnight sector. Thus, this behavior is entirely consistent with a substorm-associated particle injection event. The dashed vertical lines shown in figure 5 at 1047:48 and 1053:06 UT represent the times at which significant Pi1 and Pi2 enhancements were observed at Kakioka (see the 9th and 10th panels). Although the second (stronger) Pi2 signal clearly appears to be associated with both the energetic electron flux increase at 1984-129 and an abrupt decrease in the AL index (see 4th panel), the first Pi1 signal at 1047:48 UT does not appear to be associated with any feature in either the AL index or the geosynchronous electron fluxes. However, as shown in the second to last panel of figure 5, both Pi2 signals appear to be associated with the recovery of the plasma sheet at ISEE 1 following dropouts which began a few minutes earlier.

The global distribution of H– or X–component ground magnetic perturbations recorded during this event are shown in figure 6. As with the previous example, the black filled circles above some of the traces mark the times at which those stations passed through local magnetic midnight. The primary thing to note from this figure is that the disturbance at the time of the primary onset (1053:06 UT) was localized to the night-side of the earth and was not observed on the dayside or within the polar cap region. Therefore, this event was

not produced merely as the result of a global enhancement of the convection driven DP-2 system, but rather displays features of a typical magnetospheric substorm. Note however, that the ground magnetic perturbations did not recover substantially following the onset but instead remained perturbed until at least 13 UT. As noted above, this behavior was also observed in the AL index and in the energetic electron fluxes and is the typical signature of the "onset" of a magnetospheric convection bay (or a so-called steady magnetospheric convection interval). Despite this, all of the observations taken together indicate definitively that the event at 1053:06 UT was a substorm. Thus it appears that the substorm actually initiated the convection bay. Similar observations were reported by *McPherron et al.*, [1986] and it appears that convection bays are often activated in this manner.

In figure 7 we present a sequence of 24 images acquired with the Viking UV imager showing the evolution of the northern auroral distribution from a time before onset until well into the expansion phase. As with the previous example, only a selection of the LBH (Lyman-Birge-Hopfield) band images are shown and each image has been background and uniformity corrected before being converted to a common polar viewpoint (with 12 MLT at top center and 18 MLT at right center). Note that the increasing "fuzziness" of the images with time is due to the fact that the look direction of the Viking camera was becoming increasingly oblique as it moved away from the north polar region toward lower latitudes. Although, some activity was observed prior to the first Pi2 enhancement, the primary optical onset occurred between the fourth and fifth images of the sequence which is entirely consistent with the onset time of 1053:06 UT derived from the second Pi2 enhancement and the Los Alamos energetic particle detectors. After 1053:39 UT (fifth frame of figure 7), the auroral emissions in the midnight sector increased dramatically and a classical auroral substorm bulge developed.

All of these observations together definitively show that this event was indeed a classical magnetospheric (and auroral) substorm and was not caused solely as the result of an enhancement of the convection driven DP-2 system. In addition, from figure 5, it is clear that the onset at 1053:06 UT was not directly associated with any major fluctuation in either the IMF or the solar wind dynamic pressure. Although there was a clear northward turning of the IMF prior to the onset time, it occurred 27 minutes prior to the first Pi2 pulsation and 32 minutes prior to the second Pi2 pulsation (which was

associated with the main onset). Therefore, this feature in the solar wind can not reasonably be identified as a direct trigger for the onset of the substorm, but could very well have produced a reconfiguration of the magnetosphere which allowed some internal instability to grow.

October 31, 1986

Figure 8 shows energetic electron fluxes from three geosynchronous satellites (1982-129, 1982-019, and 1984-037), the AL index, the three components of the IMF, the solar wind dynamic pressure, and the Pi2–filtered high resolution magnetometer data from Kakioka on October 31, 1986. The locations of each of the satellites are indicated along the bottom axis. Two separate substorm intervals are evident from this plot; one occurred just after 7 UT and the other occurred after 8 UT. The only clear signature of the first interval of activity at geosynchronous orbit was the observation of a dispersed drifting population at 1982-019. This is consistent with the occurrence of an injection near local midnight, between 1984-129 and 1982-019. The onset time for this event as determined from the Pi2 pulsations observed at Kakioka was 0705:24 UT and is denoted by the first dashed vertical line in Figure 8. The second interval of substorm activity was an isolated multiple onset substorm with onset times of 0811:22 and 0829:00 UT as determined by the Pi2 pulsations at Kakioka and they are shown as the second and third dashed vertical lines in Figure 8. These onsets were clearly observed as sharp but slightly dispersed increases in the energetic electron fluxes at 1984-129 and were also observed as dispersed drifting populations at 1982-019 and 1984-037 which were located progressively farther to the east of the injection region. In addition, the AL index also displayed sharp decreases at or shortly after the onset times.

The global behavior of the ground magnetic perturbations for this event are shown in Figure 9 and are presented in the same format as Figure 3. We note that both intervals of substorm activity were associated with disturbances that were quite localized to the night-side sector and that there was no indication of a global enhancement of the DP2 current system.

From figure 8, it can be seen that, for the second interval of substorm activity, all three components of the IMF as well as the solar wind dynamic pressure were very steady for quite some time before the onset at 0811:22 UT. The first interval of substorm activity was also associated with relatively steady IMF and solar wind conditions but we note that these conditions had not persisted for very long prior to the onset.

June 15-16, 1990

In Figure 10 we present multi-point observations of an isolated substorm which occurred on June 15-16, 1990. Shown are: the energetic electron fluxes from three geosynchronous satellites (1984-129, 1989-046, and 1982-019), the X–component trace from Kiruna and the H–component trace from Leirvogur, the three components of the IMF in GSM coordinates, the solar wind dynamic pressure, and the Pi2–filtered high resolution magnetometer data from the Faroe Islands. We show the Kiruna and Leirvogur magnetometer data here because the auroral electrojet indices are presently not yet available for dates later than June of 1988. The Faroe Island station is one of seven magnetometer stations comprising the U.K. Sub-Auroral Magnetometer Network (or SAMNET).

From the Pi2 pulsations observed at the Faroe Islands, the onset of this substorm occurred at 2324 UT on June 15 which agrees quite well with the X and H traces from Kiruna and Leirvogur. The satellite 1984-129 was the closest of the three geosynchronous satellites to the east of the injection region and was situated at approximately 4 MLT at the time of onset. As can be seen, the electron fluxes at 1984-129 show a fairly dispersed increase which is consistent with its distance from the injection region. The other two satellites (1989-046 and 1982-019) were located even farther to the east of the injection region and show correspondingly increased energy dispersion. Thus, the energetic particle data show the typical signatures of a substorm–associated particle injection event. Figure 11 (the format is the same as for figure 3) also shows that the ground magnetic perturbations were consistent with a localized disturbance on the night-side rather than a global change in the DP2 current system. And finally, we see from figure 10, that the IMF and solar wind dynamic pressure were quite steady for at least 1 hour prior to the onset time.

October 19, 1990

Figure 12 shows: the energetic electron fluxes from the geosynchronous satellites, 1987-097, 1984-129, and 1989-046, the H–component traces from Lerwick and Leirvogur, the three components of the IMF in GSM coordinates, the solar wind dynamic pressure, and the Pi2–filtered high resolution H–component magnetometer data from the Faroe Islands on October 19, 1990. From both the energetic particle data and the ground magnetometer data (shown in figures 12 and 13), it can be seen that this substorm was a multiple onset substorm where the first signs of onset occurred at 0120:51

UT as determined from the Pi2 pulsations at the Faroe Islands and the energetic particle fluxes at 1987-097. This initial injection of particles seen at 1987-097 was also observed as a dispersed drifting population at 1984-129 which was situated farther to the east of the injection region. The other (later) injections observed at 1987-097 were observed in both of the other satellites as dispersed drifting populations. The D- and H-component perturbations shown in figure 13, indicate that the central meridian for this substorm was located to the west of the SAMNET array and that the stations were likely located outside (i.e. to the east of) the current wedge for the first onset at 0120:51 UT. During the second onset at about 0208 UT, it appears as though the SAMNET array was also initially outside of the current wedge but that the current wedge later expanded eastward to envelope the array.

From figure 12, it can be seen that the B_y and B_z components of the IMF were very steady for a significant amount of time prior to the onset. Thus it is clear that the onset was not associated with any significant variations in the large-scale externally imposed electric field. While a small perturbation in the IMF B_x component was observed in association with the onset (see the sixth panel), it is highly unlikely that this feature was a trigger for the substorm in large part because B_x does not contribute to the imposed electric field.

We note also from figure 12, that a relatively significant northward turning of the IMF occurred just after 4 UT and was accompanied by perturbations in B_x, B_y, and the solar wind dynamic pressure. Nevertheless, no signatures of a substorm were detected in association with this feature in either the geosynchronous energetic particle fluxes, the ground-based magnetograms or the Pi2 data from the Faroe Islands.

November 12-13, 1991

Multi-point observations of an isolated multiple onset substorm which occurred on November 11-12, 1991 are presented in Figure 14. The top three panels show the energetic electron fluxes from the geosynchronous satellites, 1987-097, 1990-095, and 1989-046, the next two panels show the H–component magnetometer trace from Kiruna and the X–component magnetometer trace from Lerwick, the sixth, seventh, and eighth panels show the three components of the IMF and the bottom two panels show the solar wind dynamic pressure and the Pi-2 filtered high resolution H–component magnetometer data from Muonio which is part of the extensive IMAGE (International Monitor for Auroral Geomagnetic Effects) magnetometer network (see Lühr

[1994] for a description of the IMAGE magnetometer network).

From the Pi2 pulsations at Muonio, the onsets were determined to have occurred at 2244:00 and 2302:40 UT, and sharp increases in the energetic electron fluxes at 1987-097 were observed following each of these times. The first of these increases was dispersionless while the second one was slightly dispersed indicating that the spacecraft had likely moved from within the injection region to just east of it over the time period between the two injections. At satellite 1990-095, which was located farther to the east, the two flux increases can be seen displaced in time and with considerably more energy dispersion, indicating that the flux increases were indeed caused by substorm associated injection events.

The X– or H–component magnetometer traces from 35 ground stations distributed throughout the polar cap region, auroral zone, and mid– and low–latitude regions are shown in figure 15 (the format is the same as that for figure 3). From this plot, it is clear that the ground magnetic perturbations in all regions were well localized to the night sector and that there is no indication of a global enhancement of the DP2 current system.

Together, these observations indicate unambiguously that this event was definitely a magnetospheric substorm and was not produced by some other type of disturbance. It is also clear from the IMP8 data shown in figure 14 that the substorm occurred during a period of extremely steady solar wind/IMF conditions and that no perturbations can be found in any of the components that could reasonably be identified as a trigger. It is also very interesting to note that this substorm occurred when the IMF B_z component was positive.

Discussion and Conclusions

We have presented detailed observations for several events that clearly show that magnetospheric substorms can indeed occur in the absence of an identifiable trigger in either the IMF or the solar wind dynamic pressure. The only significant perturbation in any of the solar wind or IMF parameters occurred during the October 19, 1990 event in which a minor perturbation in the IMF B_x component was observed near the time of onset. However, the B_x component was steady for every other case shown and none of the events presented here were associated with any significant perturbations in either the B_y or B_z component indicating that none of these events were triggered by fluctuations in the imposed solar wind electric field. As well, the comprehensive datasets compiled for each of the events indi-

cate definitively that they were true substorms and not some other type of disturbance that could potentially have been mis-identified by examining the auroral electrojet indices alone. This is an important consideration when examining intervals of steadily southward IMF because, as mentioned in the introduction, steady magnetospheric convection intervals (or magnetospheric "convection bays") are often associated with such conditions and it has been shown that large ground magnetic perturbations can occur during these events in the absence of particle injections or Pi2 pulsations (i.e. they are not substorm-related magnetic perturbations).

Although the objective of the present study was only to demonstrate that substorms can indeed occur in the absence of significant perturbations in the solar wind and IMF, an important question that remains unanswered is, how frequently do untriggered substorms occur? Unfortunately, this is a very difficult question to answer because the solar wind and IMF are ordinarily quite disturbed. As shown by *Rostoker et al.* [1988] and Hapgood et al. [1991], the IMF B_z component retains the same polarity for intervals of time greater than 2 hours only about 12-15% of the time while it retains the same polarity for time spans longer than 60 minutes only about 34% of the time. Thus, it is reasonably difficult to find events even for which the B_z component merely maintains the same polarity for significant periods of time. If, in addition, very steady conditions are required in all of the IMF components as well as in the solar wind pressure, the probability of finding candidate intervals diminishes dramatically. Nevertheless, as we have demonstrated here, they can be found. This indicates that at least some fraction of the total number of substorms that occur are the result of some process, phenomenon or mechanism intrinsic to the magnetosphere (i.e. they are "internally triggered" or "spontaneous"). This also raises the possibility that many substorms which occur during not-so-steady IMF and solar wind conditions might also be the result of an internal magnetospheric instability. Thus, although we do not suggest that all substorms are untriggered, it is important to recognize that given the variability of the solar wind/IMF system, not all associations between fluctuations and onsets are likely to be causal. As shown for the October 19, 1990 event (figure 12), it is certainly true that not all northward turnings result in substorms (see also examples presented by *McPherron et al.* [1986]).

The results of the present study are relevant to (and were in fact motivated by) the recently proposed substorm model of *Lyons* [1995a]. In this model, the onset

of the expansion phase is directly triggered by an externally imposed reduction in the large-scale electric field due to a reduction in either the B_y or B_z components of the IMF. Thus northward turnings or sharp reductions in B_y can trigger the onset in this model. Furthermore, *Lyons* [1995b] contends that "most, and perhaps all, expansions are triggered by IMF changes" of this sort implying that his model may be universally applicable. However, the results of the present study clearly indicate that triggering by reduction of the solar wind electric field certainly does not occur for all substorms. And as mentioned above, substorms may occur solely as the result of an internal magnetospheric instability much more frequently than we are able to determine. Furthermore, although we have only addressed the possibility that substorms can occur without external triggering in the present study, it is also quite likely that externally triggered events can also be found which do not result in a reduction of the large-scale electric field (e.g. a sudden increase in $|B_y|$). Therefore, we conclude that the model of *Lyons* [1995a] does not successfully account for all of the substorms that are observed – either the model is incorrect or it operates only for a subset of all substorms.

Acknowledgments. This work was conducted under the auspices of the US Department of Energy and was supported in part by the Office of Basic Energy Science. The IMP8 magnetometer data and the ISEE1 energetic particle data were obtained from the National Space Science Data Center (NSSDC) in Greenbelt, Maryland. The solar wind plasma data were obtained from the NSSDC and the MIT Space Plasma Physics Group in Cambridge, Massachusetts. The ISEE1 magnetometer data were provided by the UCLA Space Physics Data Center. The Kakioka high resolution magnetometer data and the auroral electrojet indices were provided by the World Data Center C2 for Geomagnetism, Kyoto University, Kyoto, Japan. The SAMNET data were provided by the Space Geophysics Group at the University of York and the IMAGE magnetometer network data were provided by Lasse Hakkinen of the Finnish Meteorological Institute. The magnetometer data from Hopen, Jan Mayen, Bjornoya, Ny-Aalesund and Tromso were provided by the Auroral Observatory at the University of Tromso, Norway and the magnetometer data from Kiruna were provided by the Swedish Institute of Space Physics in Kiruna, Sweden. All of the other magnetometer data were provided by the National Geophysical Data Center in Boulder, Colorado and the UCLA Space Physics Data Center. The Viking project was managed by the Swedish Space Corporation under contract to the Swedish Board for Space Activities and the UV imager was built as a project of the National Research Council of Canada.

References

Aubry, M. P., and R. L. McPherron, Magnetotail changes in relation to the solar wind magnetic field and magnetospheric substorms, *J. Geophys. Res.*, *76*, 4381, 1971.

Belian, R. D., G. R. Gisler, T. E. Cayton, and R. Christensen. High-Z energetic particles at geosynchronous orbit during the great solar proton event series of October 1989, *J. Geophys. Res.*, *97*, 16897, 1992.

Burch, J. L., Preconditions for the triggering of polar magnetic substorms by storm sudden commencements, *J. Geophys. Res.*, *77*, 5629, 1972.

Burch, J. L., Triggering of the substorm expansion phase by directional discontinuities in the interplanetary magnetic field, *EOS Trans.*, AGU, *54*, 413, 1973.

Caan, M. N., R. L. McPherron, and C. T. Russell, Substorm and interplanetary magnetic field effects on the geomagnetic tail lobes, *J. Geophys. Res.*, *80*, 191, 1975.

Caan, M. N., R. L. McPherron, and C. T. Russell, Characteristics of the association between the interplanetary magnetic field and substorms, *J. Geophys. Res.*, *82*, 4837, 1977.

Caan, M. N., R. L. McPherron, and C. T. Russell, The statistical magnetic signature of magnetospheric substorms, *Planet. Space Sci.*, *26*, 269, 1978.

Fairfield, D. H., and L. J. Cahill Jr., Transition region magnetic field and polar magnetic disturbances, *J. Geophys. Res.*, *71*, 155, 1966.

Foster, J. C., D. H. Fairfield, K. W. Ogilvie, and T. J. Rosenberg, Relationship of interplanetary parameters and occurrence of magnetospheric substorms, *J. Geophys. Res.*, *76*, 6971, 1971.

Hapgood, M. A., M. Lockwood, G. A. Bowe, and D. M. Willis, Variability of the interplanetary medium at 1 a.u. over 24 years: 1963-1986, *Planet. Space Sci.*, *39*, 411, 1991.

Higbie, P. R., R. D. Belian, and D. N. Baker, High resolution energetic particle measurements at 6.6 R_E, 1, electron micropulsations, *J. Geophys. Res.*, *83*, 4851, 1978.

Horwitz, J. L., The substorm as an internal magnetospheric instability: substorms and their characteristic time scales during intervals of steady interplanetary magnetic field, *J. Geophys. Res.*, *90*, 4164, 1985.

Kokubun, S. R., R. L. McPherron, and C. T. Russell, Triggering of substorms by solar wind discontinuities, *J. Geophys. Res.*, *82*, 74, 1977.

Koskinen, H. E. J., T. I. Pulkkinen, R. J. Pellinen, T. Bösinger, D. N. Baker, and R. E. Lopez, Characteristics of pseudobreakups, in *Proceedings of the International Conference on Substorms (ICS-1)*, 111, ESA Publications Division, Noordwijk, The Netherlands, 1992.

Lühr, H., The IMAGE magnetometer network, *STEP International, Volume 4, No. 10*, 4, 1994.

Lyons, L. R., A new theory for magnetospheric substorms, in press *J. Geophys. Res.*, April, 1995.

Lyons, L. R., Substorms: fundamental observational features, distinction from other disturbances, and external triggering, in press, *J. Geophys. Res.*, June, 1995.

McPherron, R. L., T. Terasawa, and A. Nishida, Solar wind triggering of substorm expansion onset, *J. Geomag. Geoelectr.*, *38*, 1089, 1986.

Pellinen, R. J., W. Baumjohann, W. Heikkila, V. A. Sergeev, A. G. Yahnin, G. Marklund, A. O. Melnikov, Event study on pre-substorm phases and their relation to the energy coupling between solar wind and magnetosphere, *Planet. Space Sci.*, *30*, 371, 1982.

Petrinec, S. M., and C. T. Russell, Comments on "Magnetopause shape as a bivariate function of interplanetary magnetic field B_z and solar wind dynamic pressure" by E. C. Roelof and D. G. Sibeck, *J. Geophys. Res.*, *100*, 1899, 1995.

Pudovkin, M. I., O. M. Raspopov, L. A. Dimitrieva, V. A. Troitskaya, and R. V. Shepetnov, The interrelation between parameters of the solar wind and the state of the geomagnetic field. *Ann. Geophys.*, *26*, 389, 1970.

Rostoker, G., M. Mareschal, and J. C. Samson, Response of the dayside net downward field-aligned current to changes in the interplanetary magnetic field and to substorm perturbations, *J. Geophys. Res.*, *87*, 3489, 1982.

Rostoker, G., W. Baumjohann, and C. T. Russell, A case study of the response of the magnetosphere to changes in the interplanetary medium, *J. Geophys. Res.*, *53*, 170, 1983.

Rostoker, G., Triggering of the expansive phase intensifications of magnetospheric substorms by northward turnings of the interplanetary magnetic field, *J. Geophys. Res.*, *88*, 6981, 1983.

Rostoker, G., D. Savoie, and T. D. Phan, Response of magnetosphere-ionosphere current systems to changes in the interplanetary magnetic field, *J. Geophys. Res.*, *8633*, 1988.

Troshichev, O. A., A. L. Kotikov, B. D. Bolotinskaya, and V. G. Andrezen, Influence of the IMF azimuthal component on magnetospheric substorm dynamics, *J. Geomag. Geoelectr.*, *38*, 1075, 1986.

M. G. Henderson, G. D. Reeves, R. D. Belian all at Div. of Non-proliferation and International Security, Mail Stop D436, Los Alamos National Laboratory, Los Alamos, New Mexico, 87545; J. S. Murphree at Dept. of Physics and Astronomy, University of Calgary, 2500 University Drive N.W., Calgary Alberta, Canada T2N 1N4. Internet address: mghenderson@lanl.gov. URL: http://nis-www.lanl.gov/m̃gh

HENDERSON ET AL.: SUBSTORMS WITH NO APPARENT TRIGGER

HENDERSON ET AL.: SUBSTORMS WITH NO APPARENT TRIGGER

HENDERSON ET AL.: SUBSTORMS WITH NO APPARENT TRIGGER

HENDERSON ET AL.: SUBSTORMS WITH NO APPARENT TRIGGER

HENDERSON ET AL.: SUBSTORMS WITH NO APPARENT TRIGGER

HENDERSON ET AL.: SUBSTORMS WITH NO APPARENT TRIGGER

HENDERSON ET AL.: SUBSTORMS WITH NO APPARENT TRIGGER

HENDERSON ET AL.: SUBSTORMS WITH NO APPARENT TRIGGER

HENDERSON ET AL.: SUBSTORMS WITH NO APPARENT TRIGGER
HENDERSON ET AL.: SUBSTORMS WITH NO APPARENT TRIGGER
HENDERSON ET AL.: SUBSTORMS WITH NO APPARENT TRIGGER
HENDERSON ET AL.: SUBSTORMS WITH NO APPARENT TRIGGER
HENDERSON ET AL.: SUBSTORMS WITH NO APPARENT TRIGGER
HENDERSON ET AL.: SUBSTORMS WITH NO APPARENT TRIGGER
HENDERSON ET AL.: SUBSTORMS WITH NO APPARENT TRIGGER
HENDERSON ET AL.: SUBSTORMS WITH NO APPARENT TRIGGER
HENDERSON ET AL.: SUBSTORMS WITH NO APPARENT TRIGGER

Figure 1. The three examples of "triggerless" substorm expansion phase onsets presented by McPherron et al. [1986]. The closed black circles represent values of the solar wind dynamic pressure as determined by the Los Alamos plasma instrument on the IMP8 spacecraft while the open circles connected by straight line segments represent values of the solar wind dynamic pressure as determined by the MIT plasma instrument. The large single point increases in the MIT values are likely spurious.

Figure 2. Multi-point observations of a substorm which occurred on April 14, 1986. From top to bottom the panels show: the Los Alamos energetic electron data from 3 geosynchronous satellites, the AL index, the three components of the interplanetary magnetic field vector in GSM coordinates, the solar wind dynamic pressure, Pi1 and Pi2 filtered magnetometer data from Kakioka, energetic electron data from ISEE1, and the tail field inclination angle at ISEE1.

Figure 3. H-component (or X-component) magnetograms from selected polar cap, auroral zone, and mid-latitude ground magnetic observatories on April 14, 1986. The filled (open) circles represent the time at which the corresponding ground station passed through local magnetic midnight (noon).

Figure 4. Viking ultraviolet auroral images showing the temporal development of the northern auroral distribution during a substorm which occurred on April 14, 1986. All of the images shown were acquired with camera 0 which is sensitive to the Lyman-Birge-Hopfield band emissions of N_2 (134 - 180 nm).

Figure 5. Multi-point observations of a substorm which occurred on April 13, 1986. The format is identical to that of figure 2.

Figure 6. H-component (or X-component) magnetograms from selected polar cap, auroral zone, and mid-latitude ground magnetic observatories on April 13, 1986. The filled circles represent the time at which the corresponding ground station passed through local magnetic midnight.

Figure 7. Viking ultraviolet auroral images showing the temporal development of the northern auroral distribution during a substorm which occurred on April 13, 1986. All of the images shown were acquired with camera 0 which is sensitive to the Lyman-Birge-Hopfield band emissions of N_2 (134 - 180 nm).

Figure 8. Multi-point observations of a substorm which occurred on October 31, 1986. The format is similar to that of figure 2.

Figure 9. H-component (or X-component) magnetograms from selected polar cap, auroral zone, and mid-latitude ground magnetic observatories on October 31, 1986. The filled (open) circles represent the time at which the corresponding ground station passed through local magnetic midnight (noon).

Figure 10. Multi-point observations of a substorm which occurred on June 15, 1990. From top to bottom the panels show: the Los Alamos energetic electron data from 3 geosynchronous satellites, the X and H traces from Kiruna and Leirvogur respectively, the three components of the interplanetary magnetic field vector in GSM coordinates, the solar wind dynamic pressure, and the Pi2 filtered magnetometer data from Faroes.

Figure 11. H-component (or X-component) magnetograms from selected polar cap, auroral zone, and mid-latitude ground magnetic observatories on June 15, 1990. The filled (open) circles represent the time at which the corresponding ground station passed through local magnetic midnight (noon).

Figure 12. Multi-point observations of a substorm which occurred on October 19, 1990. From top to bottom the panels show: the Los Alamos energetic electron data from 3 geosynchronous satellites, the H traces from Lerwick and Leirvogur respectively, the three components of the interplanetary magnetic field vector in GSM coordinates, the solar wind dynamic pressure, and the Pi2 filtered magnetometer data from Faroes.

Figure 13. H- and D-component magnetometer traces from the U.K. Sub-Auroral Magnetometer Network (SAMNET) on October 19, 1990.

Figure 14. Multi-point observations of a substorm which occurred on November 12, 1991. From top to bottom the panels show: the Los Alamos energetic electron data from 3 geosynchronous satellites, the X and H traces from Kiruna and Leirvogur respectively, the three components of the interplanetary magnetic field vector in GSM coordinates, the solar wind dynamic pressure, and the Pi2 filtered magnetometer data from Muonio.

Figure 15. H-component (or X-component) magnetograms from selected polar cap, auroral zone, mid-, and low-latitude ground magnetic observatories on November 12-13, 1990. The filled (open) circles represent the time at which the corresponding ground station passed through local magnetic midnight (noon).

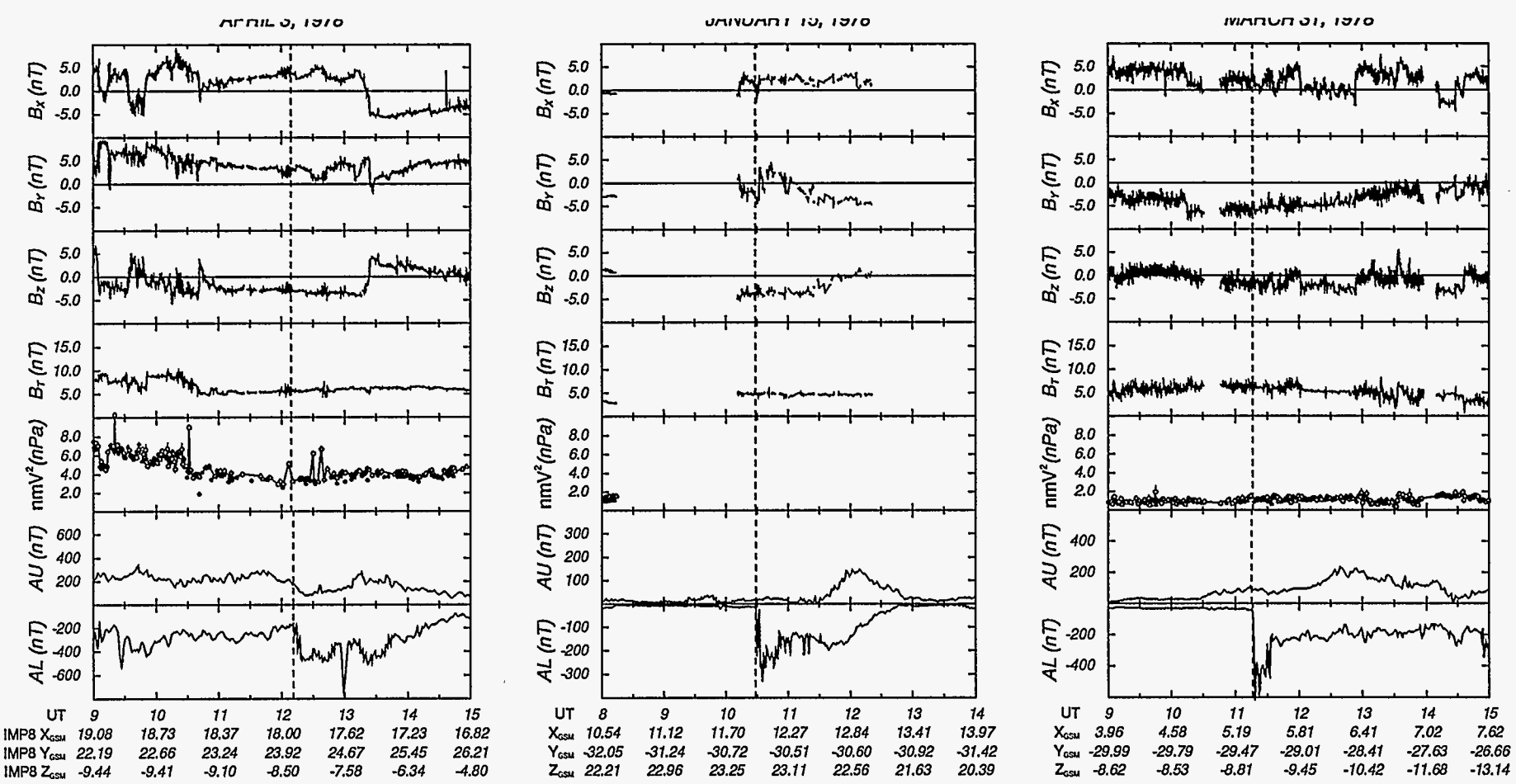
APRIL 3, 1978
JANUARY 13, 1978
MARCH 31, 1978
B_x (nT)
B_y (nT)
B_z (nT)
B_T (nT)
nmV²(nPa)
AU (nT)
AL (nT)
UT
IMP8 X_{GSM} 19.08 18.73 18.37 18.00 17.62 17.23 16.82
IMP8 Y_{GSM} 22.19 22.66 23.24 23.92 24.67 25.45 26.21
IMP8 Z_{GSM} -9.44 -9.41 -9.10 -8.50 -7.58 -6.34 -4.80
X_{GSM} 10.54 11.12 11.70 12.27 12.84 13.41 13.97
Y_{GSM} -32.05 -31.24 -30.72 -30.51 -30.60 -30.92 -31.42
Z_{GSM} 22.21 22.96 23.25 23.11 22.56 21.63 20.39
X_{GSM} 3.96 4.58 5.19 5.81 6.41 7.02 7.62
Y_{GSM} -29.99 -29.79 -29.47 -29.01 -28.41 -27.63 -26.66
Z_{GSM} -8.62 -8.53 -8.81 -9.45 -10.42 -11.68 -13.14

Figure 1

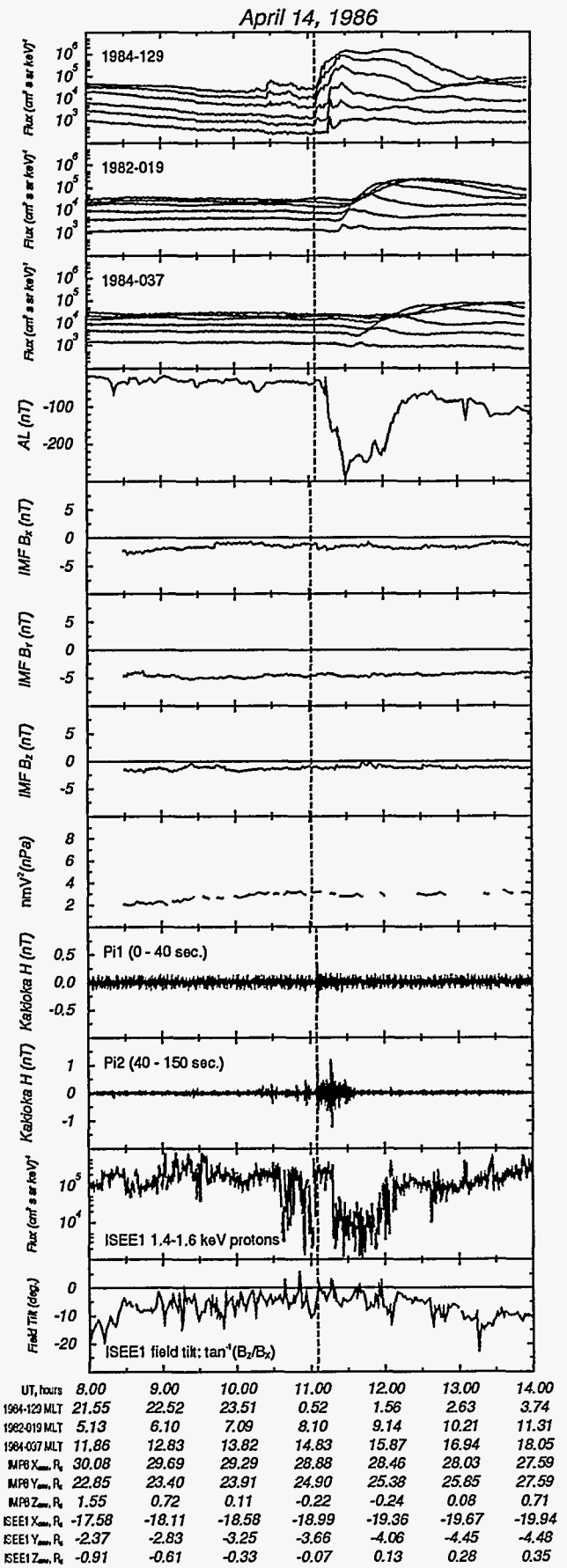

UT, hours	8.00	9.00	10.00	11.00	12.00	13.00	14.00
1984-129 MLT	21.55	22.52	23.51	0.52	1.56	2.63	3.74
1982-019 MLT	5.13	6.10	7.09	8.10	9.14	10.21	11.31
1984-037 MLT	11.86	12.83	13.82	14.83	15.87	16.94	18.05
IMP8 X_{sm}, R_E	30.08	29.69	29.29	28.88	28.46	28.03	27.59
IMP8 Y_{sm}, R_E	22.85	23.40	23.91	24.90	25.38	25.85	27.59
IMP8 Z_{sm}, R_E	1.55	0.72	0.11	-0.22	-0.24	0.08	0.71
ISEE1 X_{sm}, R_E	-17.58	-18.11	-18.58	-18.99	-19.36	-19.67	-19.94
ISEE1 Y_{sm}, R_E	-2.37	-2.83	-3.25	-3.66	-4.06	-4.45	-4.48
ISEE1 Z_{sm}, R_E	-0.91	-0.61	-0.33	-0.07	0.13	0.28	0.35

Figure 2

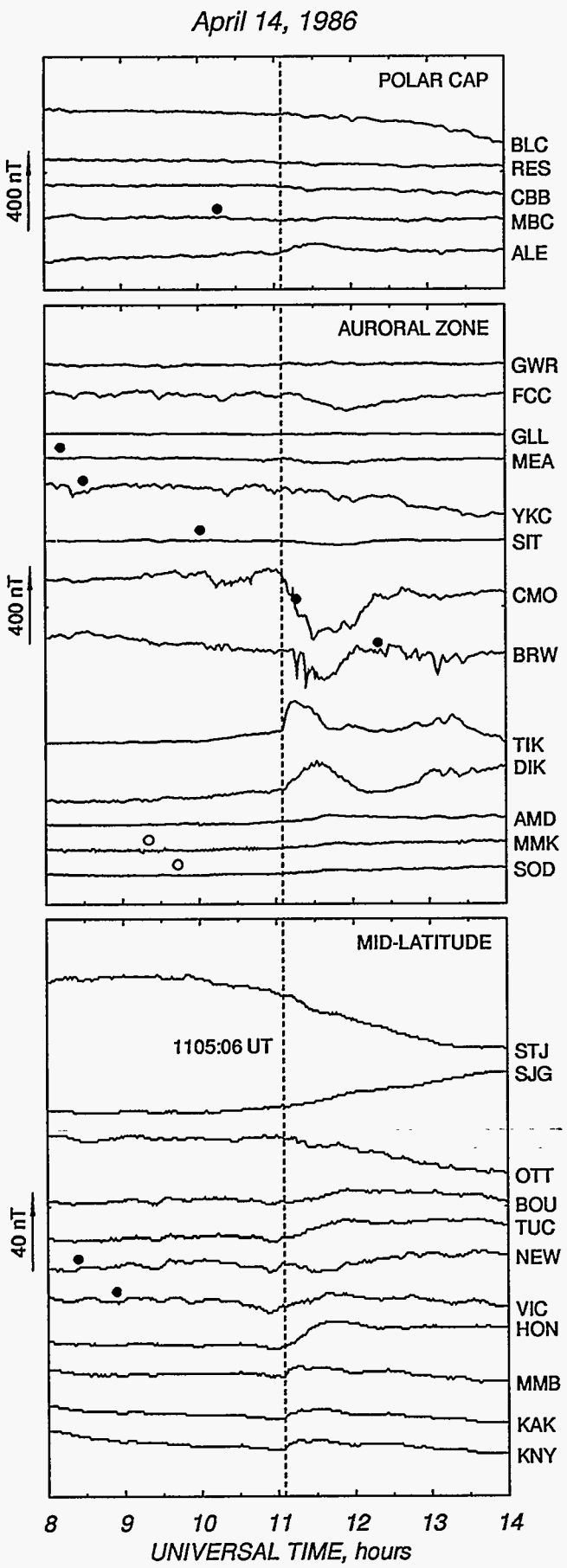
April 14, 1986
POLAR CAP
400 nT
BLC
RES
CBB
MBC
ALE
AURORAL ZONE
400 nT
GWR
FCC
GLL
MEA
YKC
SIT
CMO
BRW
TIK
DIK
AMD
MMK
SOD
MID-LATITUDE
1105:06 UT
40 nT
STJ
SJG
OTT
BOU
TUC
NEW
VIC
HON
MMB
KAK
KNY
8
9
10
11
12
13
14
UNIVERSAL TIME, hours

Figure 3

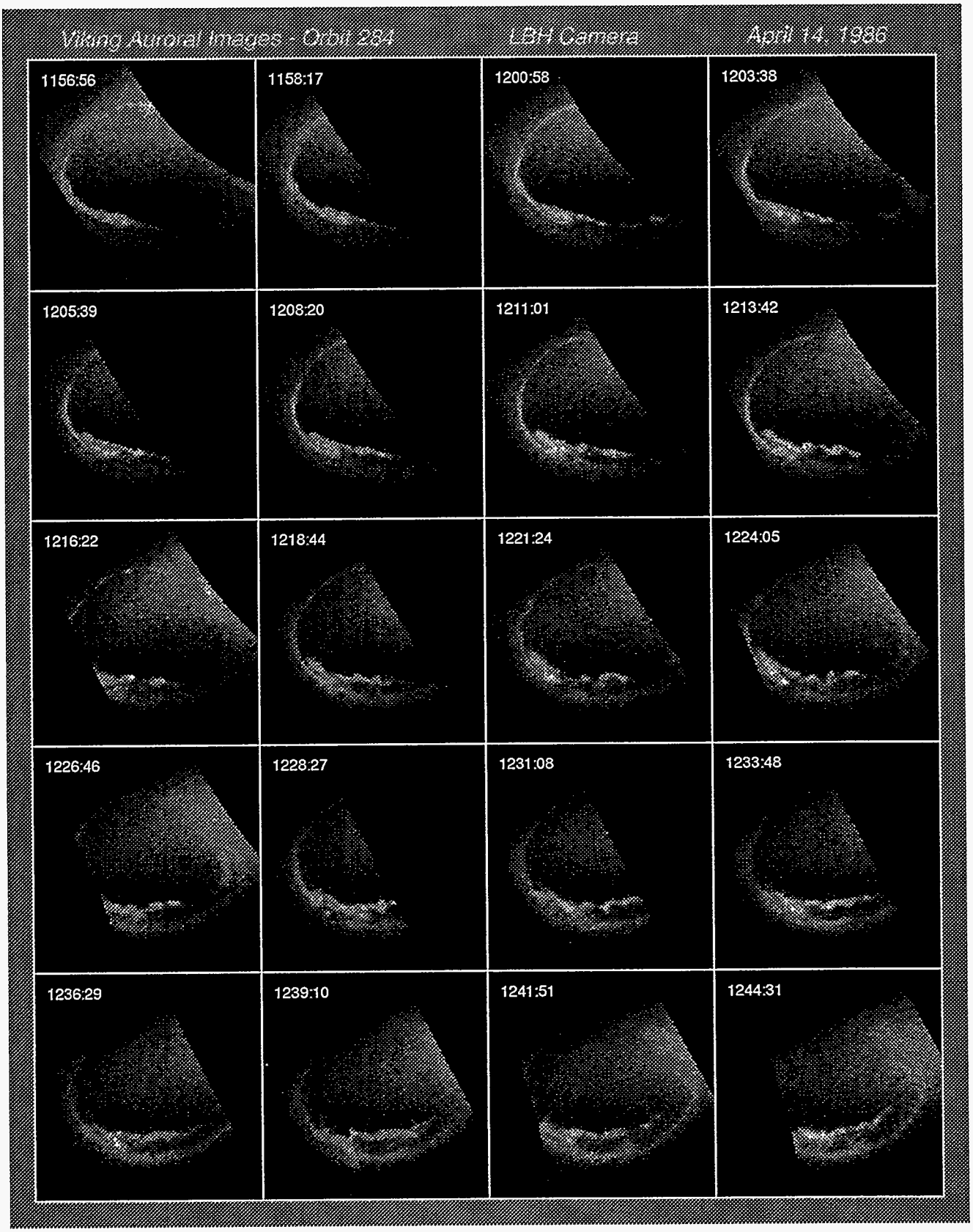
Viking Auroral Images - Orbit 284
LBH Camera
April 14, 1986
1156:56
1158:17
1200:58
1203:38
1205:39
1208:20
1211:01
1213:42
1216:22
1218:44
1221:24
1224:05
1226:46
1228:27
1231:08
1233:48
1236:29
1239:10
1241:51
1244:31

Figure 4

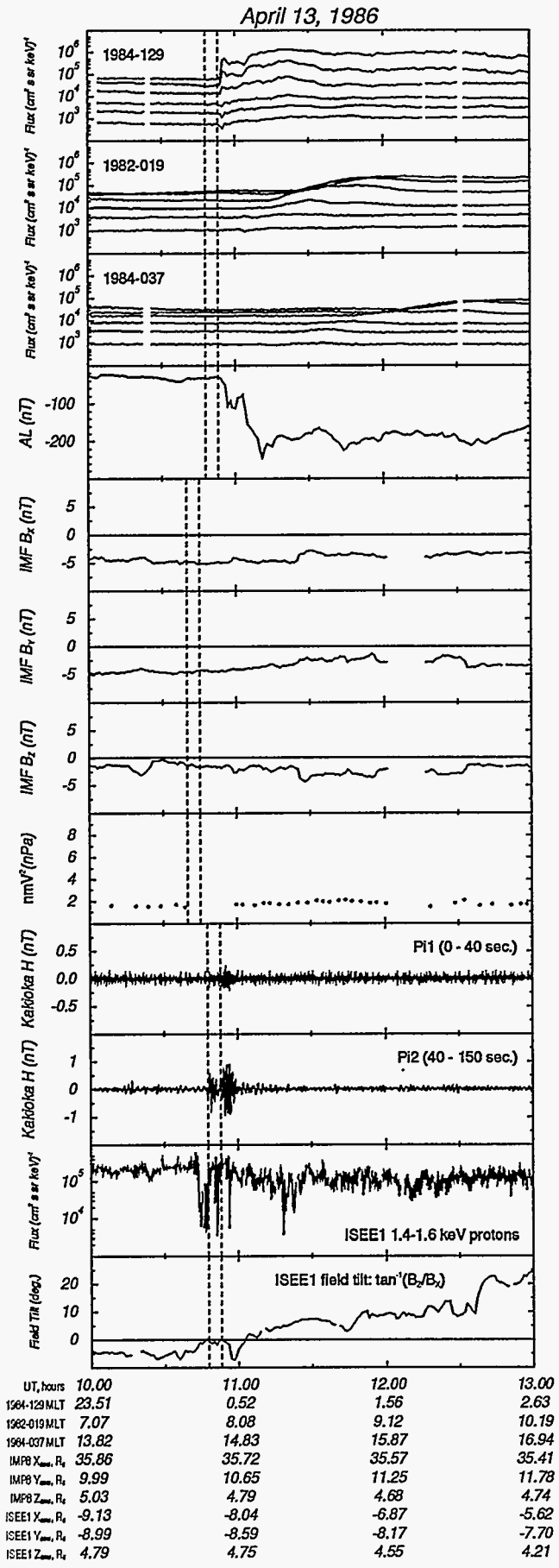

UT, hours	10.00	11.00	12.00	13.00
1984-129 MLT	23.51	0.52	1.56	2.63
1982-019 MLT	7.07	8.08	9.12	10.19
1984-037 MLT	13.82	14.83	15.87	16.94
IMP8 X_{GSE}, R_E	35.86	35.72	35.57	35.41
IMP8 Y_{GSE}, R_E	9.99	10.65	11.25	11.78
IMP8 Z_{GSE}, R_E	5.03	4.79	4.68	4.74
ISEE1 X_{GSE}, R_E	-9.13	-8.04	-6.87	-5.62
ISEE1 Y_{GSE}, R_E	-8.99	-8.59	-8.17	-7.70
ISEE1 Z_{GSE}, R_E	4.79	4.75	4.55	4.21

Figure 5

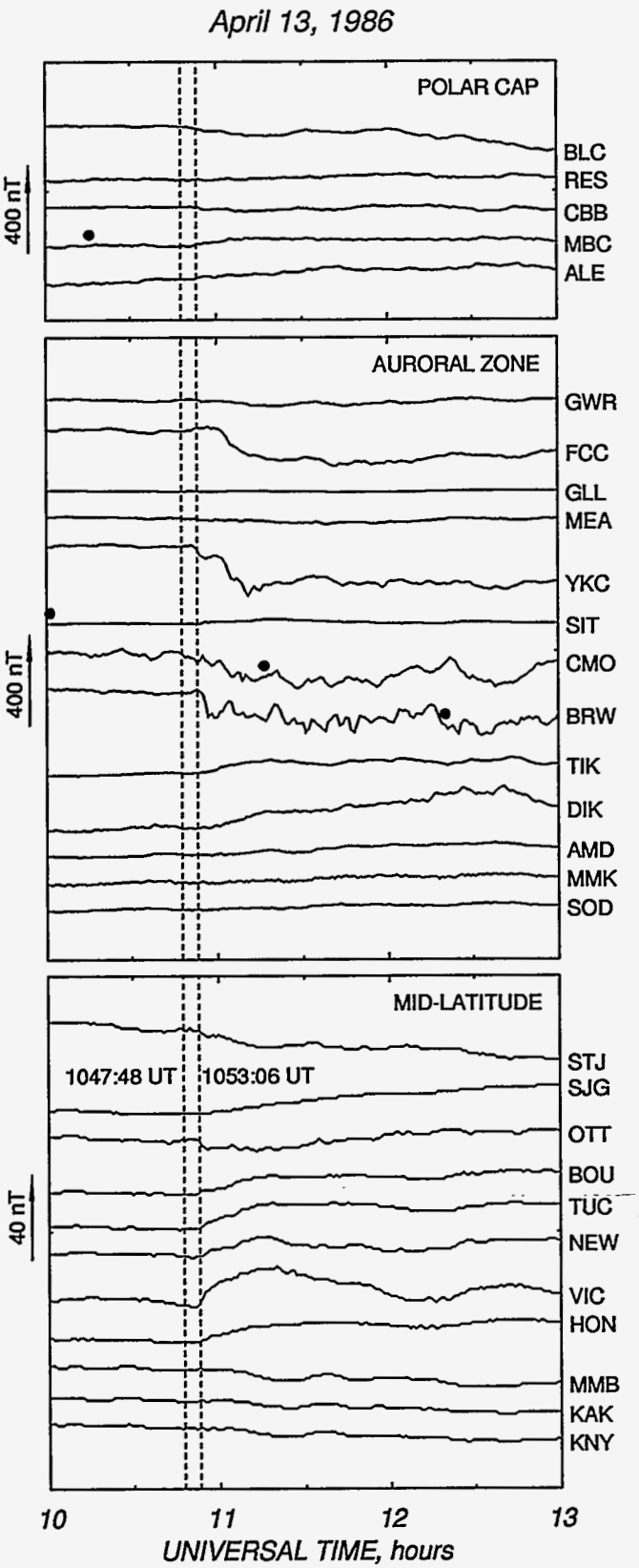
April 13, 1986
POLAR CAP
BLC
RES
CBB
MBC
ALE
400 nT
AURORAL ZONE
GWR
FCC
GLL
MEA
YKC
SIT
CMO
BRW
TIK
DIK
AMD
MMK
SOD
400 nT
MID-LATITUDE
1047:48 UT
1053:06 UT
STJ
SJG
OTT
BOU
TUC
NEW
VIC
HON
MMB
KAK
KNY
40 nT
10
11
12
13
UNIVERSAL TIME, hours

Figure 6

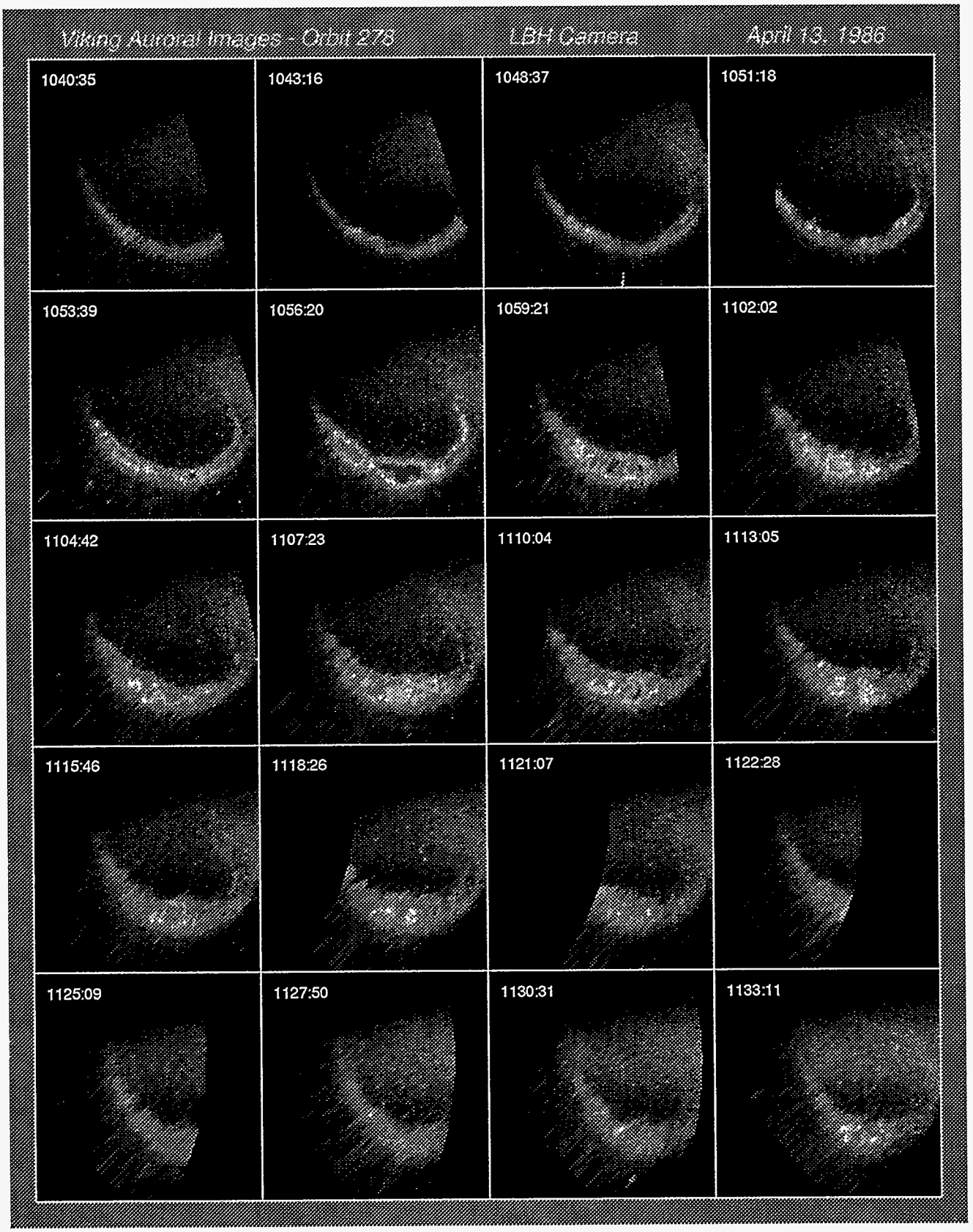
Viking Auroral Images - Orbit 278
LBH Camera
April 13, 1986
1040:35
1043:16
1048:37
1051:18
1053:39
1056:20
1059:21
1102:02
1104:42
1107:23
1110:04
1113:05
1115:46
1118:26
1121:07
1122:28
1125:09
1127:50
1130:31
1133:11

Figure 7

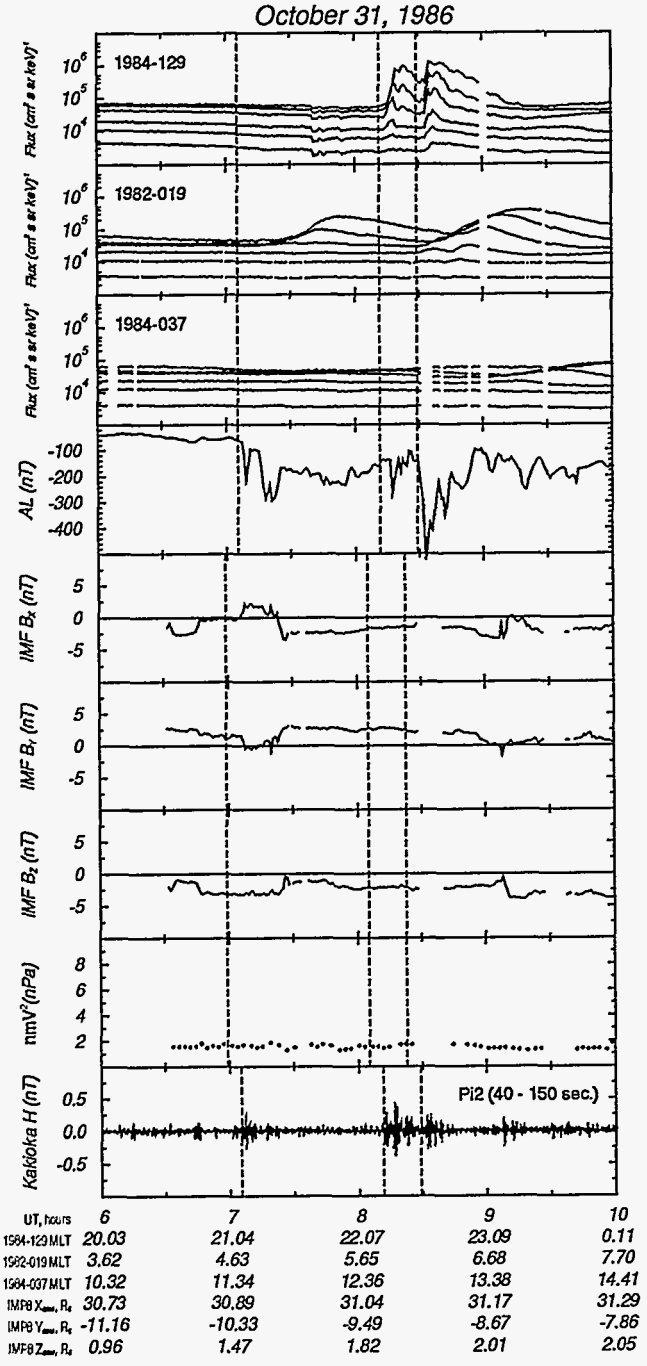
October 31, 1986
1984-129
1982-019
1984-037
Flux (cm² s sr keV)⁻¹
AL (nT)
IMF Bx (nT)
IMF By (nT)
IMF Bz (nT)
nmV²(nPa)
Kakioka H (nT)
Pi2 (40 - 150 sec.)
UT, hours 6 7 8 9 10
1984-129 MLT 20.03 21.04 22.07 23.09 0.11
1982-019 MLT 3.62 4.63 5.65 6.68 7.70
1984-037 MLT 10.32 11.34 12.36 13.38 14.41
IMP8 X, Re 30.73 30.89 31.04 31.17 31.29
IMP8 Y, Re -11.16 -10.33 -9.49 -8.67 -7.86
IMP8 Z, Re 0.96 1.47 1.82 2.01 2.05

Figure 8

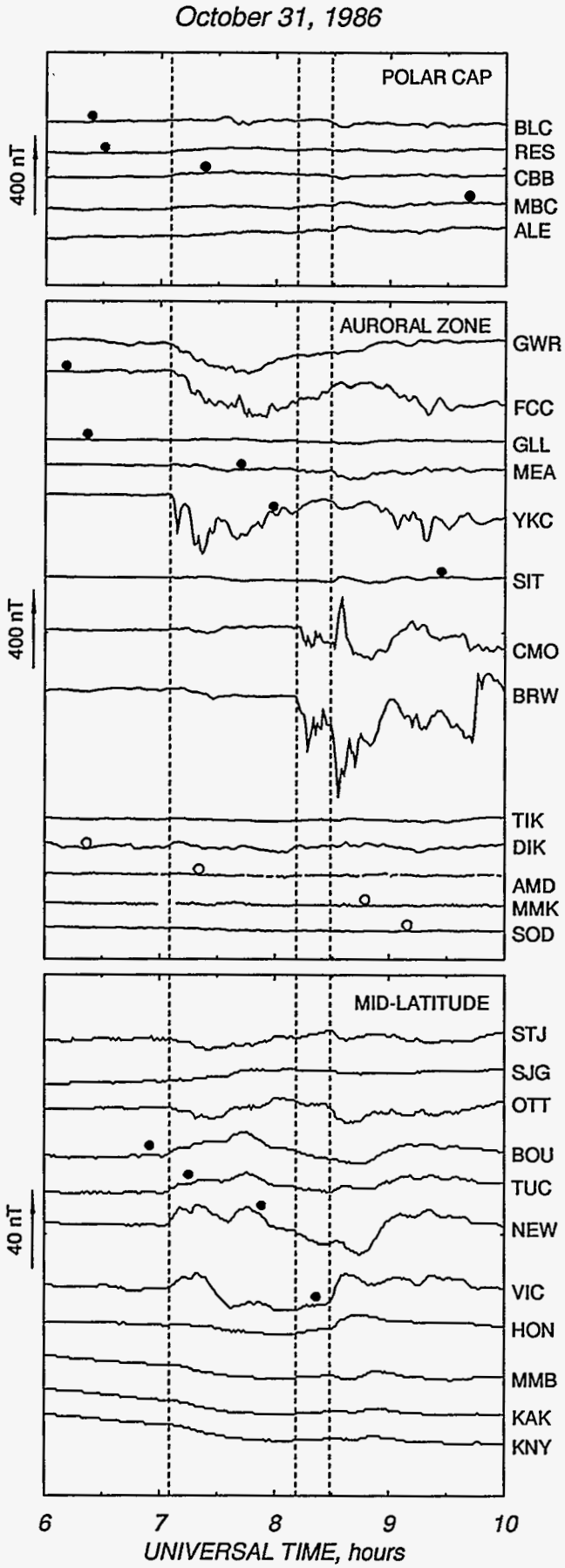
October 31, 1986
POLAR CAP
BLC
RES
CBB
MBC
ALE
400 nT
AURORAL ZONE
GWR
FCC
GLL
MEA
YKC
SIT
CMO
BRW
TIK
DIK
AMD
MMK
SOD
400 nT
MID-LATITUDE
STJ
SJG
OTT
BOU
TUC
NEW
VIC
HON
MMB
KAK
KNY
40 nT
6
7
8
9
10
UNIVERSAL TIME, hours

Figure 9

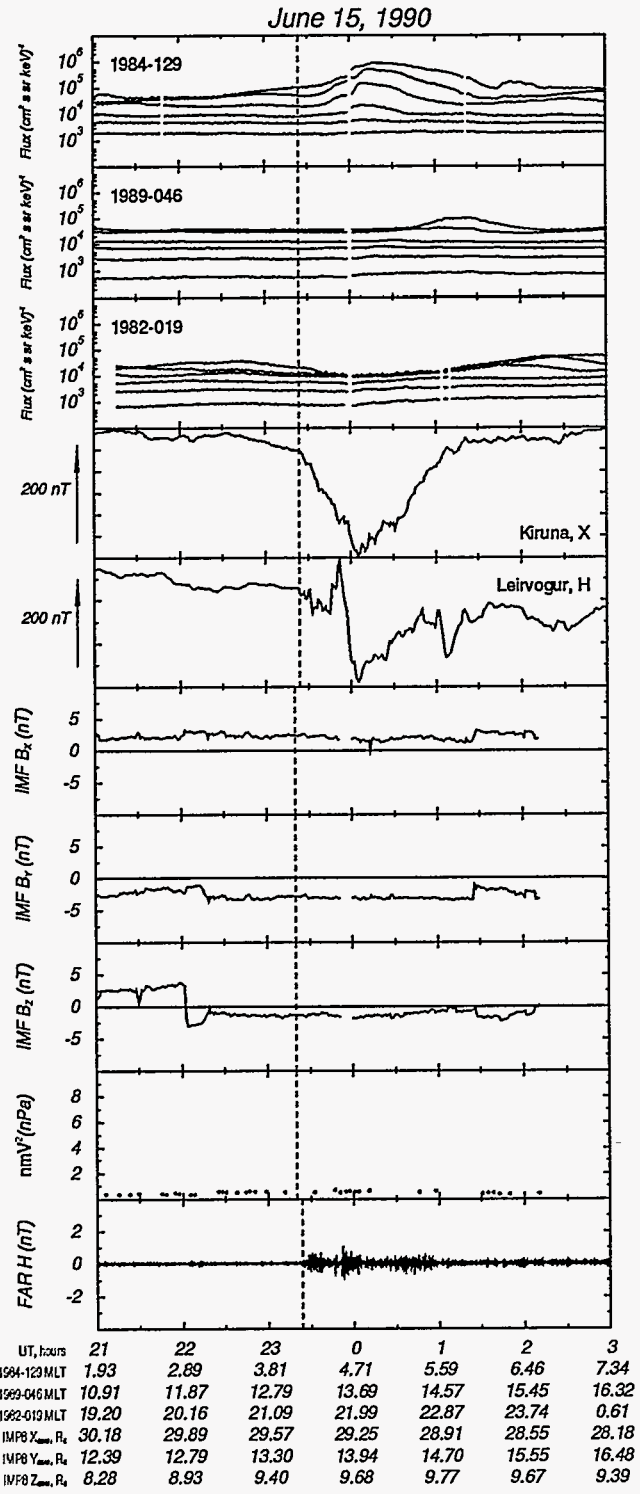

UT, hours	21	22	23	0	1	2	3
1984-129 MLT	1.93	2.89	3.81	4.71	5.59	6.46	7.34
1989-046 MLT	10.91	11.87	12.79	13.69	14.57	15.45	16.32
1982-019 MLT	19.20	20.16	21.09	21.99	22.87	23.74	0.61
IMP8 X_{GSM}, R_E	30.18	29.89	29.57	29.25	28.91	28.55	28.18
IMP8 Y_{GSM}, R_E	12.39	12.79	13.30	13.94	14.70	15.55	16.48
IMP8 Z_{GSM}, R_E	8.28	8.93	9.40	9.68	9.77	9.67	9.39

Figure 10

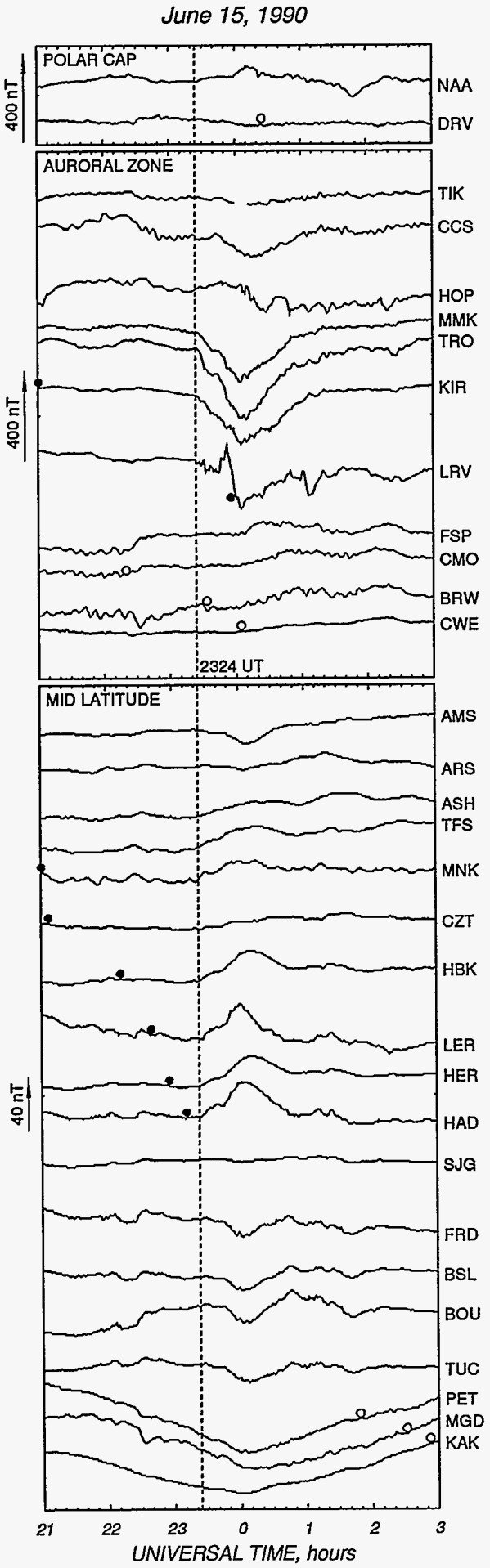
June 15, 1990
POLAR CAP
400 nT
NAA
DRV
AURORAL ZONE
TIK
CCS
HOP
MMK
TRO
KIR
LRV
FSP
CMO
BRW
CWE
2324 UT
MID LATITUDE
AMS
ARS
ASH
TFS
MNK
CZT
HBK
LER
HER
HAD
SJG
FRD
BSL
BOU
TUC
PET
MGD
KAK
40 nT
21
22
23
0
1
2
3
UNIVERSAL TIME, hours

Figure 11

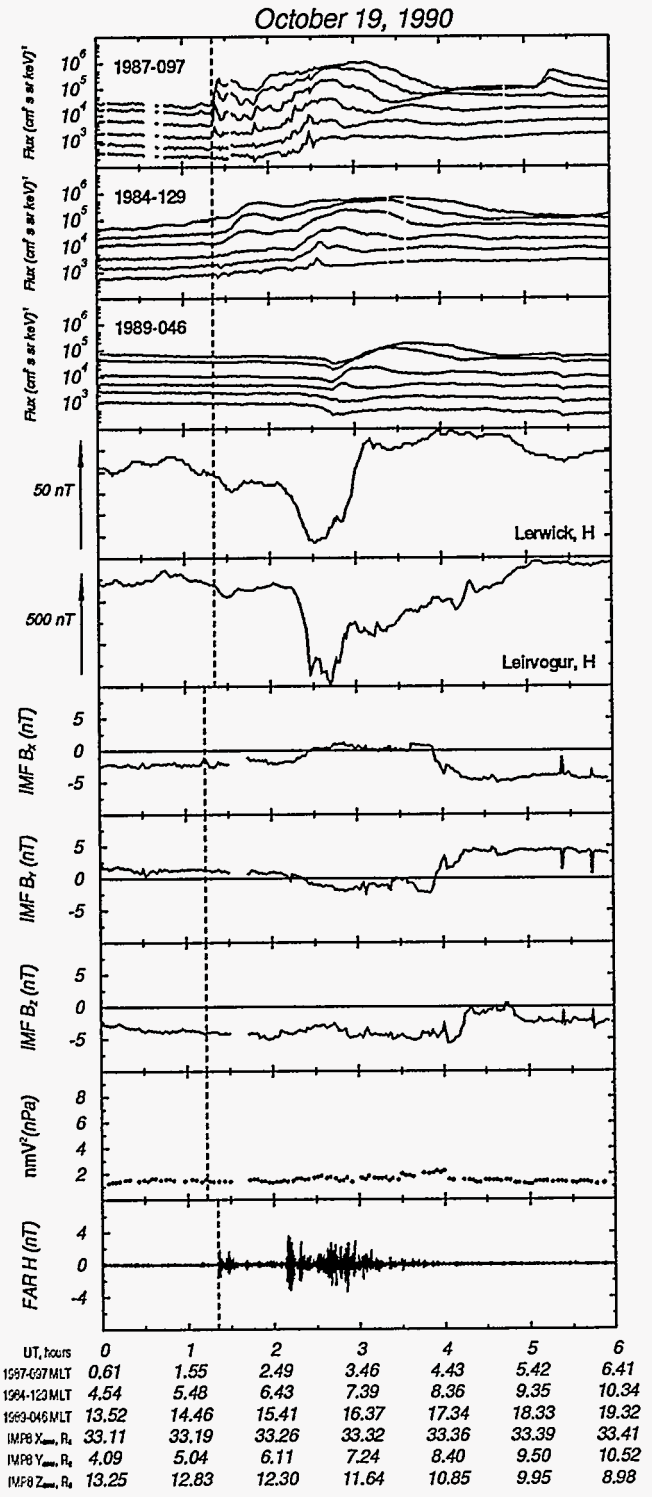

UT, hours	0	1	2	3	4	5	6
1987-097 MLT	0.61	1.55	2.49	3.46	4.43	5.42	6.41
1984-129 MLT	4.54	5.48	6.43	7.39	8.36	9.35	10.34
1989-046 MLT	13.52	14.46	15.41	16.37	17.34	18.33	19.32
IMP8 X GSM, Re	33.11	33.19	33.26	33.32	33.36	33.39	33.41
IMP8 Y GSM, Re	4.09	5.04	6.11	7.24	8.40	9.50	10.52
IMP8 Z GSM, Re	13.25	12.83	12.30	11.64	10.85	9.95	8.98

Figure 12

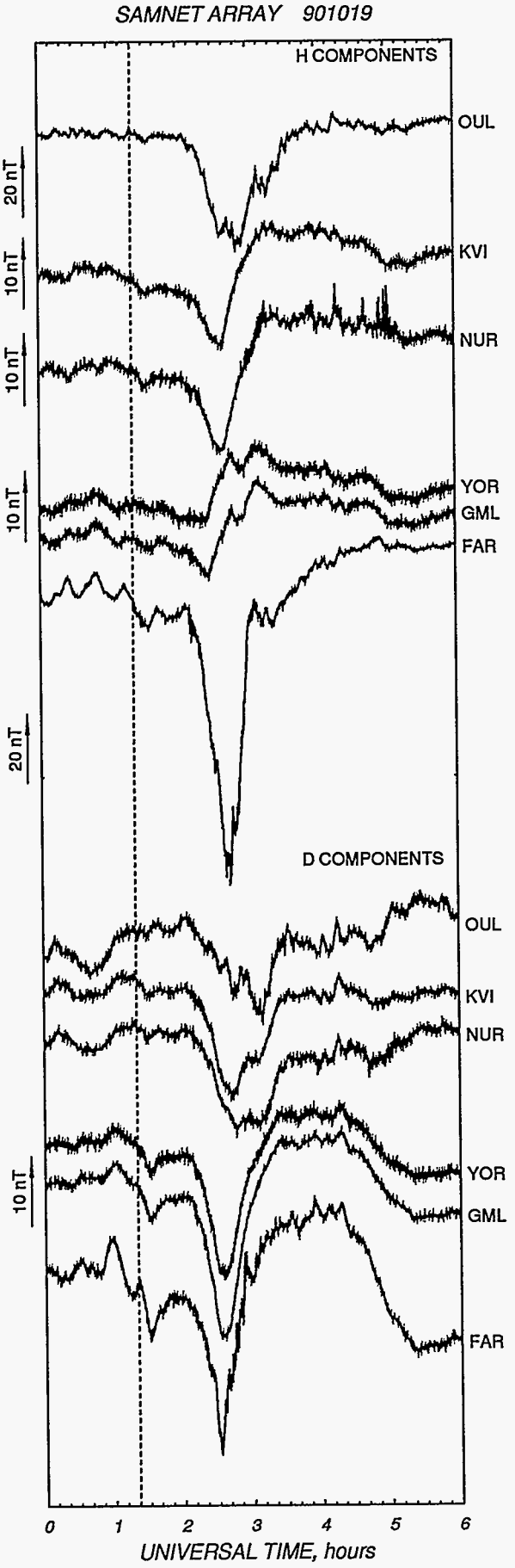
SAMNET ARRAY 901019
H COMPONENTS
OUL
KVI
NUR
YOR
GML
FAR
20 nT
10 nT
10 nT
10 nT
20 nT
D COMPONENTS
OUL
KVI
NUR
YOR
GML
FAR
10 nT
0
1
2
3
4
5
6
UNIVERSAL TIME, hours

Figure 13

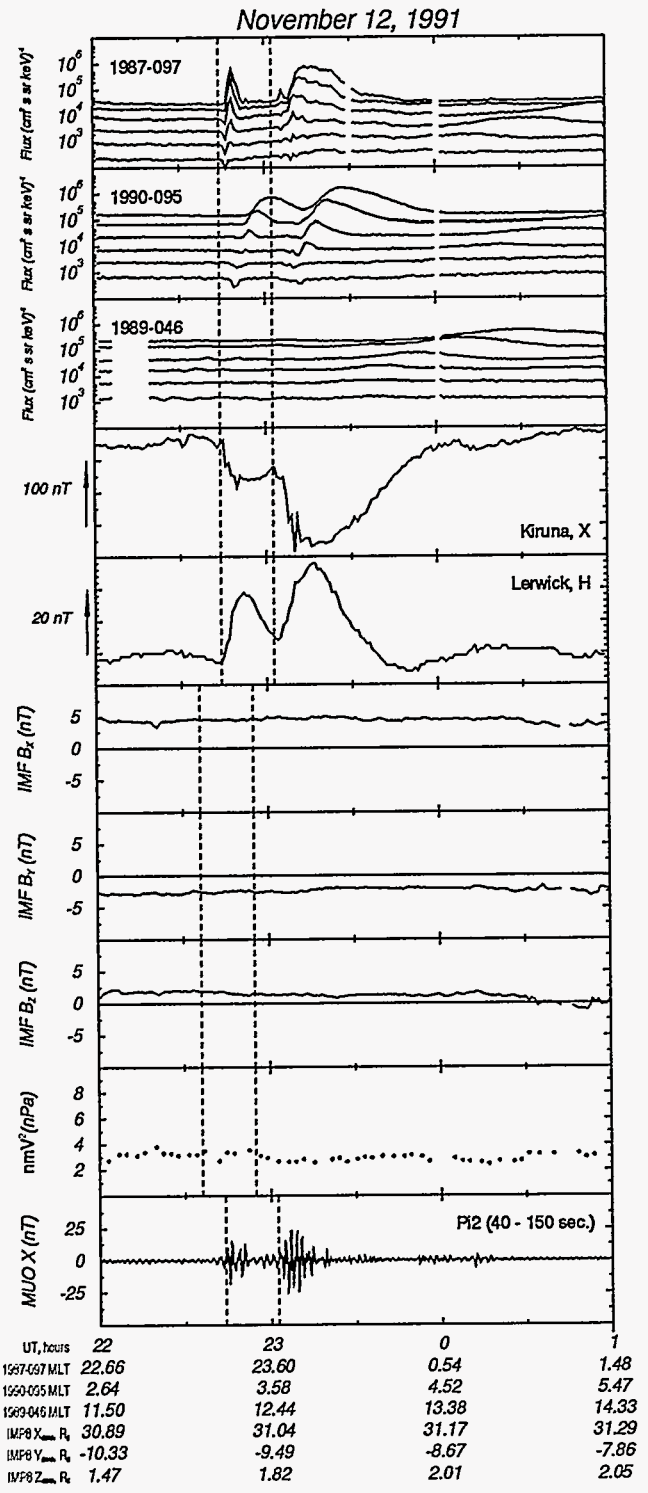
November 12, 1991
1987-097
1990-095
1989-046
Flux (cm² s sr keV)⁻¹
100 nT
Kiruna, X
20 nT
Lerwick, H
IMF Bx (nT)
IMF By (nT)
IMF Bz (nT)
nmV²(nPa)
MUO X (nT)
Pi2 (40 - 150 sec.)
UT, hours 22 23 0 1
1987-097 MLT 22.66 23.60 0.54 1.48
1990-095 MLT 2.64 3.58 4.52 5.47
1989-046 MLT 11.50 12.44 13.38 14.33
IMF Bx Re 30.89 31.04 31.17 31.29
IMF By Re -10.33 -9.49 -8.67 -7.86
IMF Bz Re 1.47 1.82 2.01 2.05

Figure 14

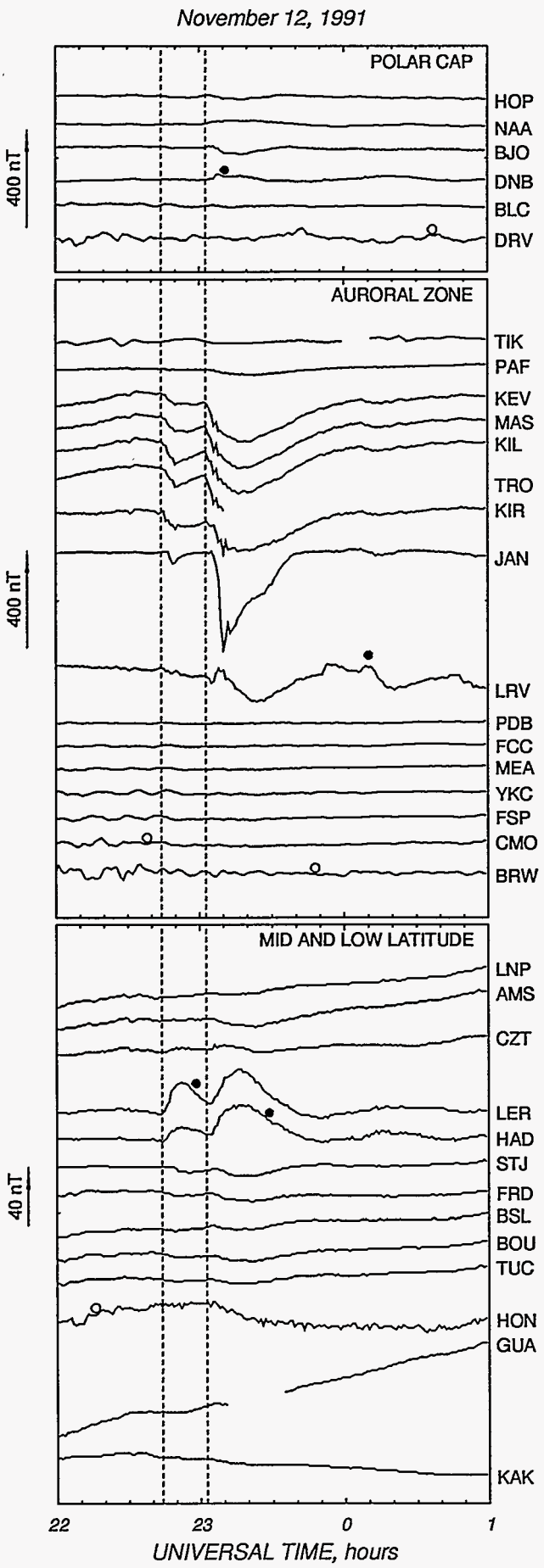
November 12, 1991
POLAR CAP
HOP
NAA
BJO
DNB
BLC
DRV
400 nT
AURORAL ZONE
TIK
PAF
KEV
MAS
KIL
TRO
KIR
JAN
LRV
PDB
FCC
MEA
YKC
FSP
CMO
BRW
400 nT
MID AND LOW LATITUDE
LNP
AMS
CZT
LER
HAD
STJ
FRD
BSL
BOU
TUC
HON
GUA
KAK
40 nT
22
23
0
1
UNIVERSAL TIME, hours

Figure 15

Table 1. Differential Energy Bands for the Los Alamos Energetic Electron Data. Note that the energies given are nominal and that small differences exist between the various spacecraft. See Higbie et al. [1978] and Belian et al. [1992] for more detailed descriptions of the CPA and SOPA detectors respectively.

Channel	CPA[a]	SOPA[b]
1	30-45 keV	50-75 keV
2	45-65 keV	75-105 keV
3	65-95 keV	105-155 keV
4	95-140 keV	155-225 keV
5	140-200 keV	225-320 keV
6	200-300 keV	320-500 keV

[a]CPA detectors were flown on: 1982-019, 1984-037, 1984-129 and 1987-097.

[b]SOPA detectors were flown on: 1989-046 and 1990-095.

Table 2. Onsets Examined in This Study

Date	Onset Time(s) *(Universal Time)*
April 13, 1986	10:47:48
	10:53:06
April 14, 1986	11:05:06
October 31, 1986	07:05:24
	08:11:22
	08:29:00
June 15, 1990	23:24:00
October 19, 1990	01:20:51
November 11, 1991	22:44:00
	23:02:40

Table 3. Ground Magnetic Observatories Used in this Study

Observatory	Code	geo. lat. *(deg.)*	geo. lon. *(deg.)*	mag. lat. *(deg.)*	mag. lon. *(deg.)*
Amserdam Island	AMS	-37.8	77.6	-48.4	136.7
Arti	ARS	56.4	58.6	48.7	133.0
Ashkabad	ASH	38.0	58.1	30.1	129.5
Baker Lake	BLC	64.3	264.0	71.6	334.0
Barrow	BRW	71.4	203.7	72.7	252.2
Bay St. Louis	BSL	30.4	270.6	38.2	343.7
Bjornoya	BJO	74.5	19.0	70.2	110.6
Boulder	BOU	40.1	254.8	47.1	325.8
Cape Chelyuskin	CCS	77.7	104.3	69.7	169.3
Cape Wellen	CWE	66.2	190.2	65.8	244.6
College	CMO	64.9	212.2	67.6	268.4
Crozet	CZT	-46.4	51.9	-51.1	105.1
Daneborg	DNB	74.3	339.8	74.8	78.6
Dumont Durville	DRV	-66.7	140.0	-79.3	239.3
Faroes[a]	FAR	62.1	353.0	61.8	78.0
Fort Churchill	FCC	58.8	265.9	66.1	337.1
Fort Simpson	FSP	61.7	238.8	67.5	301.8
Fredricksburg	FRD	38.2	282.6	45.8	356.7
Glenmore[a]	GML	57.2	356.3	56.7	78.5
Guam	GUA	13.6	144.9	4.1	215.0
Hartland	HAD	51.0	355.5	50.9	75.3
Hartebeesthoek	HBK	-25.9	27.7	-26.8	89.3
Hermanus	HER	-34.4	19.2	-32.9	79.1
Honolulu	HON	21.3	202.0	21.5	273.0
Hopen	HOP	76.5	25.0	71.5	117.3
Jan Mayen	JAN	70.9	8.7	68.0	98.8
Kakioka	KAK	36.2	140.2	28.0	207.3
Kevo[b]	KEV	69.8	27.0	64.9	112.5
Kilpisjarvi[b]	KIL	69.1	20.7	64.9	106.9
Kiruna	KIR	67.8	20.4	63.8	105.8
Kvistaberg[a]	KVI	59.5	17.6	56.1	98.9
Leirvogur	LRV	64.2	338.3	65.8	65.3
Lerwick	LER	60.1	358.8	59.1	82.3
Lunping	LNP	25.0	121.2	14.4	189.5
Masi[b]	MAS	69.5	23.7	65.0	109.6
Meanook	MEA	54.6	246.7	61.0	314.0
Minsk	MNK	54.5	27.9	49.9	106.1
Muonio[b]	MUO	68.0	23.5	63.6	108.5
Nordli[a]	NOR	64.4	13.4	61.3	97.7
Nurmijarvi[a]	NUR	60.5	24.7	56.2	105.5
Ny-Aalesund	NAA	78.8	11.9	74.9	112.3
Ottawa	OTT	45.4	284.4	52.8	359.1

Table 3. (continued)

Observatory	Code	geo. lat. *(deg.)*	geo. lon. *(deg.)*	mag. lat. *(deg.)*	mag. lon. *(deg.)*
Oulu[a]	OUL	65.1	25.9	60.5	108.7
Pamatai	PPT	-17.6	210.4	-16.5	289.1
Petropavlovsk	PET	52.9	158.4	47.9	221.3
Port-Aux-France	PAF	-49.4	70.2	-58.0	122.8
Poste de la Baleine	PDB	55.3	282.2	62.6	357.4
San Juan	SJG	18.1	293.8	26.3	7.7
St Johns	STJ	47.6	307.3	53.6	25.0
Tbilisi	TFS	41.7	44.8	35.3	118.0
Tixie Bay	TIK	71.6	129.0	64.5	188.9
Tromso	TRO	69.7	18.9	65.7	106.0
Tucson	TUC	32.2	249.2	38.8	320.6
Yellowknife	YKC	62.4	245.5	68.8	309.9
York[a]	YOR	54.0	359.0	53.3	79.6

[a]From the SAMNET array.
[b]From the IMAGE array.